

IsoME: Streamlining High-Precision Eliashberg Calculations

Eva Kogler,¹ Dominik Spath,¹ Roman Lucrezi,^{1,2} Hitoshi Mori,³
Zien Zhu,⁴ Zhenglu Li,⁴ Elena R. Margine,³ and Christoph Heil^{1,*}

¹*Institute of Theoretical and Computational Physics, Graz University of Technology, NAWI Graz, 8010, Graz, Austria*

²*Department of Materials and Environmental Chemistry, Stockholm University, SE-10691 Stockholm, Sweden*

³*Department of Physics, Applied Physics, and Astronomy,*

Binghamton University-SUNY, Binghamton, New York 13902, USA

⁴*Mork Family Department of Chemical Engineering and Materials Science,
University of Southern California, Los Angeles, California 90089, USA*

(Dated: March 6, 2025)

This paper introduces the Julia package IsoME, an easy-to-use yet accurate and robust computational tool designed to calculate superconducting properties. Multiple levels of approximation are supported, ranging from the basic McMillan-Allen-Dynes formula and its machine learning-enhanced variant to Eliashberg theory including static Coulomb interactions derived from *GW* calculations, offering a fully *ab initio* approach to determine superconducting properties, such as the critical superconducting temperature (T_c) and the superconducting gap function (Δ). We validate IsoME by benchmarking it against various materials, demonstrating its versatility and performance across different theoretical levels. The findings indicate that the previously held assumption that Eliashberg theory overestimates T_c is no longer valid when μ^* is appropriately adjusted to account for the finite Matsubara frequency cutoff. Furthermore, we conclude that the constant density of states (DOS) approximation remains accurate in most cases. By unifying multiple approximation schemes within a single framework, IsoME combines first-principles precision with computational efficiency, enabling seamless integration into high-throughput workflows through its T_c search mode. This makes IsoME a powerful and reliable tool for advancing superconductivity research.

INTRODUCTION

Since the discovery of superconductivity by Onnes in 1911 [1], unraveling the nature of the superconducting phase has remained a central challenge in condensed matter physics. A significant milestone was achieved by the Bardeen-Cooper-Schrieffer (BCS) theory [2], which provided the first microscopic description of weak-coupling superconductors. This concept was later generalized by the Migdal-Eliashberg (ME) theory [3, 4], treating the problem in a many-body perturbation approach, to account for effects such as retardation and strong coupling. Building on these *ab-initio* methods, simplified semi-empirical equations for the critical temperature (T_c) such as the McMillan [5] and Allen-Dynes [6] equations were formulated as practical approximations. While these equations often provide accurate estimates for T_c , they do not capture the full complexity of the underlying physics. They are limited to predict T_c alone, neglecting all other superconducting properties relevant for applications, such as single-photon detection [7], Josephson junctions [8], and qubits [9].

Therefore, until today, ME theory, along with density functional theory for superconductors (SCDFT) [10–12], remains the state-of-the-art framework for describing superconductors.

Although ME theory has been available since the 1960s, progress in the field of superconductivity has historically been driven by experimental discoveries. This stems primarily from the computational complexity of the two essential steps required to predict novel superconductors: first, determining

the (meta-)stable crystal structure, and second, accurately calculating their superconducting properties. The exponential growth in computational power over the past decades, however, coupled with the development of highly efficient and accurate numerical codes, has led to a paradigm shift towards the discovery of superconductors *in silico* [13].

The impact of refined computational methods has been strikingly demonstrated with the advent of high-pressure hydride superconductors [14–16]. The breakthrough began in 2014 with H_3S , for which theory predicted a record-high T_c [17], soon followed by its independent experimental realization [18]. Since then, every hydride superconductor realized experimentally has first been predicted theoretically, underscoring the reliability of computational approaches [13, 15]. Notable examples include LaH_{10} [19, 20], YH_6 [19, 21], and LaBeH_8 [22–24]. These successes stress that carefully conducted crystal structure predictions, combined with accurate T_c computations, serve as trustworthy guides for experimental efforts.

With this work, we aim to further facilitate the prediction and description of superconductors by introducing the very efficient and highly accurate, open-source Julia [25] package IsoME [26]. IsoME enables the calculation of superconducting properties at different levels of approximation within the framework of isotropic ME theory, as schematically depicted in Fig. 1. In its default setup, IsoME solves the isotropic ME equations with just a^2F - the Eliashberg spectral function - as input, which can be obtained with modern density functional theory/density functional perturbation theory (DFT/DFPT) codes. For more advanced calculations, additional inputs such as the electronic density of states (DOS) and screened Coulomb interaction W can be incorporated, allowing for a fully *ab-initio* treatment of superconductivity [27–

* Corresponding author: christoph.heil@tugraz.at

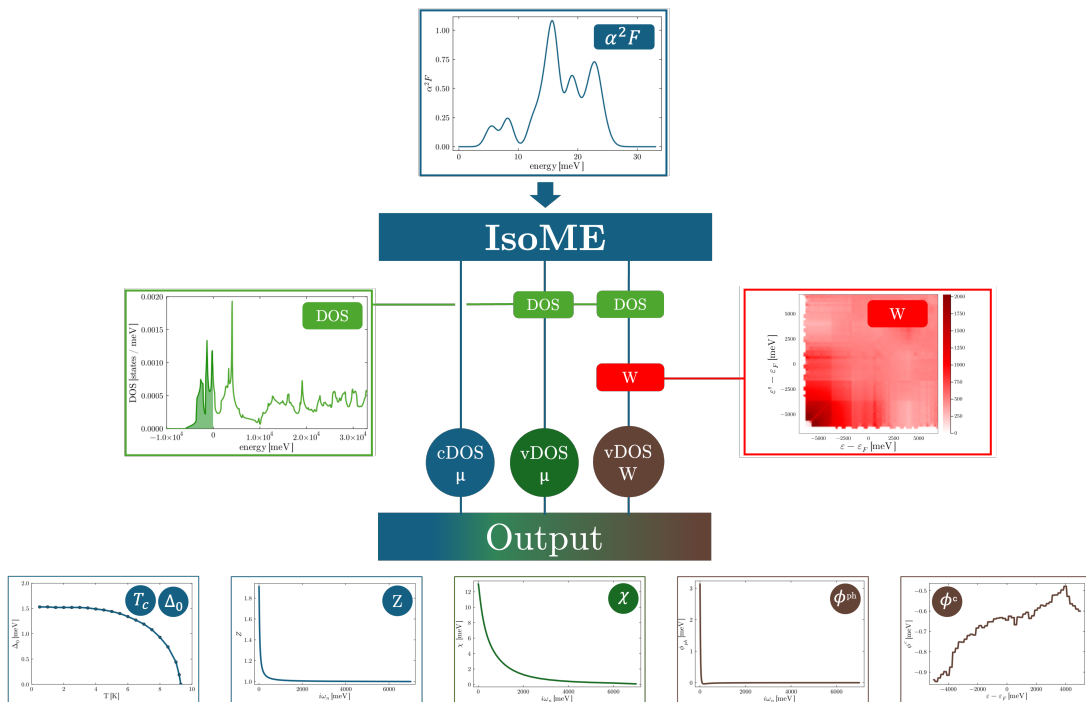


Figure 1: Flowchart of the IsoME code showing how input and output files are associated with each level of theory. The $\alpha^2 F(\omega)$ file is the only input needed for the constant DOS (cDOS) approximation and is also required for all other computations. The electronic DOS and screened Coulomb interaction are specifically needed for variable DOS (vDOS) and W calculations, respectively. As output, T_c and the components of the self-energy are returned.

32]. Furthermore, IsoME supports a T_c search mode, eliminating the need for explicit temperature specification and enhancing efficiency in high-throughput calculations. Combined with the different levels of theory, this provides valuable information to guide experimental efforts.

The paper is structured as follows. In Sec. I, we describe the functionalities of IsoME, evaluate its performance, and present insights from our benchmarking study. Sec. II reviews the ME theory and details the isotropic equations corresponding to the highest level of theory implemented in IsoME. Finally, Sec. III provides the computational details of our calculations.

I. RESULTS AND DISCUSSION

IsoME

The IsoME code package [26] is highly flexible, enabling detailed analysis across the following multiple levels of approximation for studying the properties of the superconducting phase, schematically depicted in Fig. 1.

The set of equations (13a)-(13c), (15a), and (15b), as detailed in Sec. II, constitutes currently the most complete and rigorous implementation to solve the isotropic Migdal-Eliashberg theory completely from first-principles, taking into account the full energy dependence of the electronic DOS and the screened Coulomb interaction, giving access to not only

T_c , but also to the superconducting gap function Δ , the mass renormalization Z , the energy shift χ , and thus the full Nambu-Gor'kov Green's function \hat{G} [33]. Throughout this text, we will refer to this level of theory as vDOS+W (for *variable DOS with static Coulomb W*). A future version of IsoME currently in development will allow to perform the transformation from Matsubara to real frequency space using Nevanlinna analytic continuation [34].

The IsoME package further allows to efficiently solve two simplified forms of Eliashberg theory, employing two common approximations.

(i) μ approximation: The computation of W is a challenging and resource-intensive task in itself. For cases where this is not possible or desired, we have implemented the option to use a single scalar μ^* - the Morel-Anderson pseudopotential [35] - instead of the full energy-dependent W . It is defined as

$$\mu^* = \frac{\mu}{1 + \mu \ln\left(\frac{\epsilon_{el}}{\hbar\omega_{ph}}\right)}, \quad (1)$$

where μ is the Fermi-surface averaged W , ω_{ph} is a characteristic cutoff frequency for the phonon-induced interaction, and ϵ_{el} is a characteristic electronic energy scale. When used within the McMillan-Allen-Dynes formula and its modifications, a μ_{AD}^* between 0.1 and 0.16 has been found to be appropriate for most conventional superconductors when compared to experiments [6]. Within ME theory, however, the corresponding phonon energy scale is given by the Matsubara frequency cutoff ω_c , thus μ^* within the Eliashberg formalism

(μ_E^*) needs to scale accordingly with ω_c [32].

Within IsoME, users can specify either μ , μ_{AD}^* , or μ_E^* . In case μ_{AD}^* is supplied, the corresponding μ_E^* is determined using [32]

$$\frac{1}{\mu_E^*} = \frac{1}{\mu_{AD}^*} + \ln\left(\frac{\omega_{ph}}{\omega_c}\right). \quad (2)$$

Employing this approximation results in a simplified set of equations, as provided in [Eqs. (6)-(9)] of the Supplemental Material (SM) [36]. Throughout the paper, this approximation will be abbreviated as vDOS+ μ .

(ii) *cDOS approximation*: IsoME also supports the constant DOS (cDOS) approximation, in which case the Eliashberg equations simplify significantly as $\chi = 0$ and the chemical potential μ_F is constant. The corresponding set of equations is provided in Eqs. (12) and (13) of the SM [36]. We will refer to this approximation as cDOS+ μ . At this lowest level of theory, illustrated by the blue color in the flowchart, only the Eliashberg spectral function $\alpha^2F(\omega)$ is required as input, making IsoME suitable for integration into high-throughput workflows. To further support such applications, we have implemented a dedicated T_c search mode for all levels of theory. This mode automatically determines T_c to the nearest Kelvin without the need for explicit temperature specification.

We also want to mention at this point that considerable effort has been invested in selecting default parameters that, in most cases, ensure both computational efficiency and robust convergence. Further details can be found in Sec. II.

IsoME can be installed with the Julia package manager. Computations are started by handing over the input arguments to the `EliashbergSolver()` function. As mentioned above, for the cDOS+ μ approximation, only the $\alpha^2F(\omega)$ file is required.

```

1 using IsoME
2
3 inp = arguments(
4     a2f_file = "path-to-a2f-file",
5     outdir   = "path-to-output-directory",
6 )
7
8 EliashbergSolver(inp)

```

All other input flags have predefined default values which are contained within the custom data type `arguments()`. For further information, we refer to the documentation of the package. We want to stress at this point that IsoME can automatically detect the different file formatting for QUANTUM ESPRESSO (QE) [37–39], EPW [40, 41] and BERKELEYGW [42–44]. Automatic compatibility with other DFT/DFPT/GW packages is currently under development.

For more advanced calculations, the electronic DOS can also be provided, resulting in the vDOS+ μ variant, depicted by the green color in Fig. 1. The most rigorous approach - vDOS+W - incorporates both the variable DOS (vDOS) and the full static Coulomb interaction $W(\varepsilon, \varepsilon')$, as presented on the right-hand side of the flowchart. To initiate any of these variants, it is necessary to include the additional input files and to set the respective flags.

```

1 using IsoME
2
3 inp = arguments(
4     a2f_file   = "path-to-a2f-file",
5     dos_file   = "path-to-dos-file",
6     Weep_file  = "path-to-W-file",
7     outdir     = "path-to-output-directory",
8     cDOS_flag  = 0, # 0 = vDOS, 1 = cDOS
9     include_weep = 1, # 0 = mu, 1 = W
10 )
11
12 EliashbergSolver(inp)

```

IsoME includes, in principle, a fourth level of approximation that combines the static Coulomb interaction $W(\varepsilon, \varepsilon')$ with the cDOS approximation, as detailed in [Eqs. (1)-(5)] of the SM [36]. However, this variant is not recommended, as it requires the same input data as the vDOS+W approach while being less rigorous and offering no notable computational advantage.

The outputs produced by IsoME include the critical temperature T_c , the superconducting gap function Δ , and the renormalization function Z . When using the vDOS+ μ or vDOS+W approaches, the energy shift χ and the phononic/electronic contributions to the anomalous self-energy $\phi^{ph/c}$ are also provided (see the bottom panel of Fig. 1). Moreover, IsoME automatically generates a plot of the gap function at the zeroth Matsubara frequency, Δ_0 , which approximates the gap on the real frequency axis. Fig. 2 presents the temperature dependence of Δ_0 for LaBeH₈: the individual dots correspond to the calculated temperature points, while the dashed line is the result of a curve fitting using the functional form known from BCS theory $\Delta_0(T) = \Delta_0(0) \tanh\left(\frac{\pi k_B T_c}{\Delta_0(0)} \sqrt{a\left(\frac{T_c}{T} - 1\right)}\right)$, with fitting parameters a , $\Delta_0(0)$, and T_c . Regardless of the selected approximation, the package also evaluates the critical temperature using both the McMillan-Allen-Dynes formula (Supplementary Eq. (17) [5, 6, 45]) and its machine learning-enhanced variant (Supplementary Eq. (21) [46]).

Benchmarking

Offering the above-mentioned range of approximations, IsoME maintains high efficiency and performance. Calculations can be performed on standard PCs within a reasonable timeframe, as shown in Tab. I, which lists the runtimes for single-temperature calculations at 1, 10, and 100 K for the hydride superconductor LaBH₈ [23] across the three theoretical levels available in IsoME. Computation time grows as temperature decreases, due to the increasing number of Matsubara frequency points at lower temperatures. We implemented a sparse-sampling scheme [47–49], to speed up the calculations at very low temperatures.

Furthermore, IsoME features an automatic T_c search mode, which further enhances computational efficiency. Fig. 3a illustrates the runtime required to determine T_c for Nb, LaBeH₈ and NbC. In the case of Nb, IsoME calculated the T_c within 28 s using the cDOS+ μ method, within 91 s with the vDOS+ μ method, and within 287 s with the vDOS+W method. For LaBeH₈, the vDOS+ μ /W calculations took slightly longer than for Nb due to the broader temperature search range. All

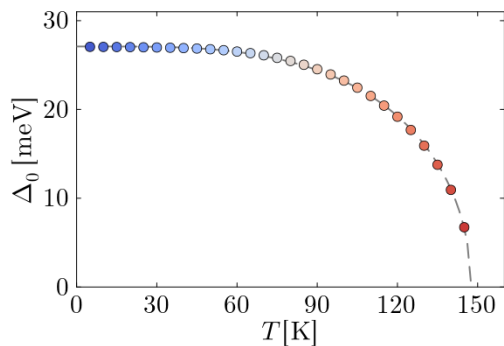


Figure 2: Temperature evolution of the superconducting gap Δ_0 for LaBeH₈ as computed by IsoME. The markers indicate the actual calculation points, and the dashed curve represents the fitted function described in the main text.

Table I: Computation runtimes of IsoME for LaBH₈ at three temperatures for the three theoretical levels.

	1 K	10 K	100 K
cDOS+ μ	138 s	0.8 s	0.1 s
vDOS+ μ	346 s	10.7 s	1.9 s
vDOS+W	370 s	28.0 s	15.0 s

these calculations were performed on a single core of an off-the-shelf workstation.

To quantitatively validate our computational framework, we first performed benchmark calculations of T_c 's (to the nearest Kelvin) for an extensive set of materials using the default value of $\mu^* = 0.12$. This approach allowed us to sidestep the considerable computational cost associated with a full W calculation. The results, presented in Tab. I of the SM [36], show excellent agreement across the various levels of approximation and with experimental data.

Encouraged by these promising benchmarks, we subsequently computed both W and μ using BERKELEYGW [42–44] for several particularly interesting materials, thereby obtaining fully *ab initio* results from ME theory. The set of materials comprises elementary, binary, and ternary superconductors, including high-pressure hydrides. The results are summarized in Tab. II.

Elementary superconductors: Elementary superconductors typically consist of only a few atoms per unit cell, making them amenable to both detailed experimental characterization and accurate theoretical modeling. This is confirmed by our benchmark study on Nb, Al, and Tc, where all approximations yield very similar T_c values. For instance, when comparing calculations with constant and variable DOS for Nb - which exhibits a pronounced peak at the Fermi level - we observe a deviation of only 1 K. Furthermore, incorporating an energy-dependent Coulomb interaction $W(\varepsilon, \varepsilon')$ does not notably alter the computed T_c for these materials. Overall, our results agree closely with experimental measurements, with one notable exception: Technetium. Here, reproducing the experimental T_c of 11 K would require a larger effective Coulomb

parameter than the calculated static value of $\mu = 0.21$. This discrepancy is consistent with the findings of Ref. [54], which suggest that spin fluctuations - absent in our Coulomb-only treatment - may further suppress T_c in Technetium.

While the semi-empirical equations provide accurate estimations for T_c 's of elementary superconductors, they do not provide any insight into the nature of the superconducting state. ME theory, on the other hand, offers a detailed description of the self-energy components, which we show as an example for Nb in panels (b) and (c) of Fig. 3. The following characteristics are observed across all materials considered: At moderately high Matsubara frequencies, the mass renormalization function Z quickly approaches unity, while the phonon contribution to the order parameter, ϕ^{ph} , vanishes. In contrast, the energy shift χ decays to zero only at significantly higher frequencies. Moreover, the electronic component of the order parameter, ϕ^e , exhibits distinct features that reflect the influence of both the DOS and the energy-dependent Coulomb interaction $W(\varepsilon, \varepsilon')$.

Disordered binary alloy superconductors: Alloy superconductors, including NbN, NbTi, TiN, and NbC, are of particular interest due to their prevalence in numerous technological applications. However, unlike elementary superconductors, modeling disordered binary superconductors poses significant challenges, often attributable to vacancies that result in an off-stoichiometry phase rather than a 1:1 ratio. To benchmark IsoME, we approximated the structure of the alloys by a 1:1 stoichiometry, which leads to an overestimation of T_c across all levels of approximation. The effect is particularly pronounced for TiN, where the calculated T_c is three times higher than the experimental one. For NbC, the calculated T_c aligns more closely with experiments, particularly when using a standard μ_{AD}^* value of 0.12 instead of the computed one (see Tab. I in the SM [36]). For alloyed systems, the limitation arises not from the theoretical treatment of superconductivity itself but from the inadequate representation of the disordered crystal structure. To accurately capture defects, large supercells are necessary, rendering simulations prohibitively costly and time-consuming. Methods such as the supercell approach used for NbTi in Ref. [55] or the ECQCA framework [56] provide potential solutions, yet these refinements are beyond the scope of this work.

Hydrides: Building on Ashcroft's prediction that atomic hydrogen under high pressure could have a record-breaking high T_c [57], hydrogen-based superconductors have attracted significant attention. Some compounds achieve superconductivity at or near room temperature but at unfeasibly high pressures for practical applications. Considerable efforts are being made to realize a hydrogen superconductor stable under near-ambient conditions. Modeling such materials accurately is particularly challenging, as hydrogen compounds can exhibit properties distinct from other conventional superconductors, including exceptionally strong electron-phonon coupling, unique electronic features at the Fermi level, and quantum anharmonic effects [13].

Indeed, the hydrides included in our calculations exhibit the most pronounced discrepancy between different levels of theory. In contrast, for non-hydrides, both the McMillan-

Table II: Comparison of resulting T_c for different levels of theory within IsoME. T_c^{AD} , T_c^{ML} , $T_c^{\text{E, cdos}, \mu}$, $T_c^{\text{E, vdos}, \mu}$, $T_c^{\text{E, vdos}, W}$, and T_c^{exp} are the critical superconducting temperatures within McMillan-Allen-Dynes, the machine learned improvement of it, Migdal-Eliashberg constant DOS and variable DOS using μ as input, Migdal-Eliashberg variable DOS including static Coulomb interactions, and the experimental value, respectively. The given μ value was calculated within GW . The asterisk indicates alloyed materials, where the crystal structure and 1:1 stoichiometry used to model the material may differ from the experimental one.

Compound	μ (from W)	T_c^{AD} [K]	T_c^{ML} [K]	$T_c^{\text{E, cdos}, \mu}$ [K]	$T_c^{\text{E, vdos}, \mu}$ [K]	$T_c^{\text{E, vdos}, W}$ [K]	T_c^{exp} [K]
Nb	0.38	9	9	9	8	7	9.1-9.5 [50]
Al	0.26	1	1	1	1	1	1.2 [50]
Tc	0.21	16	17	16	16	16	8.2-9.3-11.1 [50]
NbC	0.17	17	17	16	15	16	12.8* [51]
TiN	0.13	18	17	17	16	17	5.6* [50]
H ₃ S (200 GPa)	0.29	225	255	237	216	211	172-184 [18]
YH ₆ (200 GPa)	0.20	208	237	231	226	227	208-214 [52]
LaBeH ₈ (100 GPa)	0.16	130	139	141	140	140	104 [53]
LaBH ₈ (50 GPa)	0.13	147	161	152	154	158	-

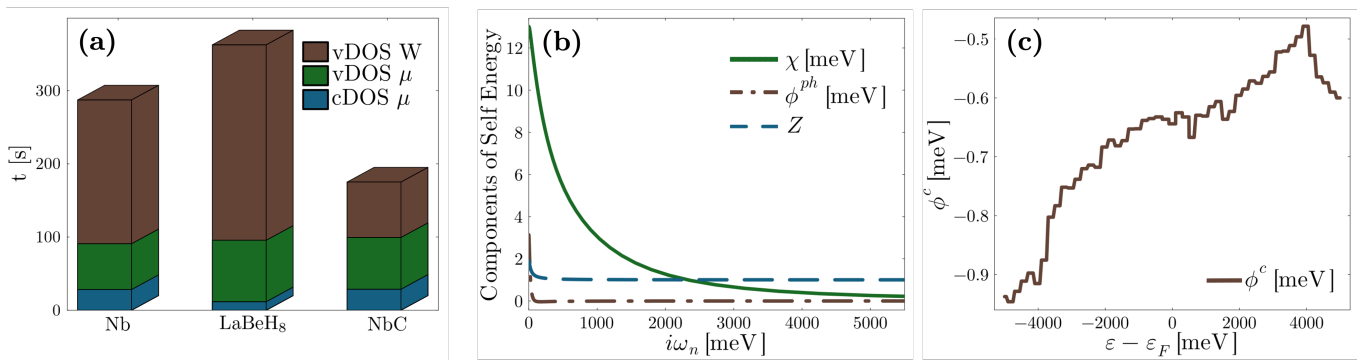


Figure 3: Duration of T_c calculations and self-energy components of Nb. Panel (a) illustrates the runtime for the T_c search mode for the different levels of theory for Nb, LaBeH₈, and NbC. In panel (b), the energy shift χ (solid green line), the renormalization function Z (dashed blue line), and the phononic part of the order parameter ϕ^{ph} (dash-dotted brown line) are shown. The electronic part of the order parameter ϕ^c is displayed in panel (c) as solid brown line.

Allen-Dynes equation and its machine-learned improved variant agree with ME theory within 2 K. However, hydrides differ from the materials used to fit the AD equation, leading to deviations of 19, 10, and 11 K for YH₆, LaBeH₈, and LaBH₈ respectively, when compared to the vDOS+W approximation, while the T_c^{ML} model aligns with ME calculations within a few percent. Interestingly, for H₃S, the difference for T_c^{AD} is 19 K, whereas the machine-learned formula deviates by 44 K from $T_c^{\text{E, vdos}, W}$. This underscores the importance of *ab-initio* methods to predict superconductors, as novel materials may exhibit properties not (well) represented in certain datasets. Additionally, *first-principles* methods give more insights into the underlying physics, such as access to the gap function Δ and other components of the self-energy (see Fig. 2 and 3).

It is important to note that perfect agreement between calculated and experimental T_c values for hydride superconductors is not expected. Our calculations are based on ideal, high-symmetry structures with perfect three-dimensional periodicity (i.e., single crystals). In contrast, experimental syntheses - especially under extreme conditions - often yield samples with

impurities, vacancies, and other types of disorder that can alter superconducting properties. Moreover, quantum anharmonic effects, which are particularly significant in these materials, are not included in our current approach [58–61]. Despite these differences, the strong agreement between our calculated T_c values and experimental observations underscores the robustness of our theoretical framework.

The results obtained for constant or variable DOS using the μ approximation differ only by a few percent for YH₆, LaBeH₈, and LaBH₈. H₃S, however, shows a pronounced peak at the Fermi level, where the assumption of a constant DOS around the Fermi level is no longer valid. As a result, a difference of 21 K is observed, where the T_c calculated using vDOS+ μ is closer to the experimental value. The largest deviation in T_c between vDOS+ μ and vDOS+W occurs for H₃S and LaBH₈, where $W(\varepsilon, \varepsilon')$ varies strongly at the Fermi energy, leading to a difference of 5 and 4 K, respectively. In general, taking into account the full energy-dependent Coulomb repulsion had little influence on most materials in our benchmark study. However, a more pronounced impact is expected

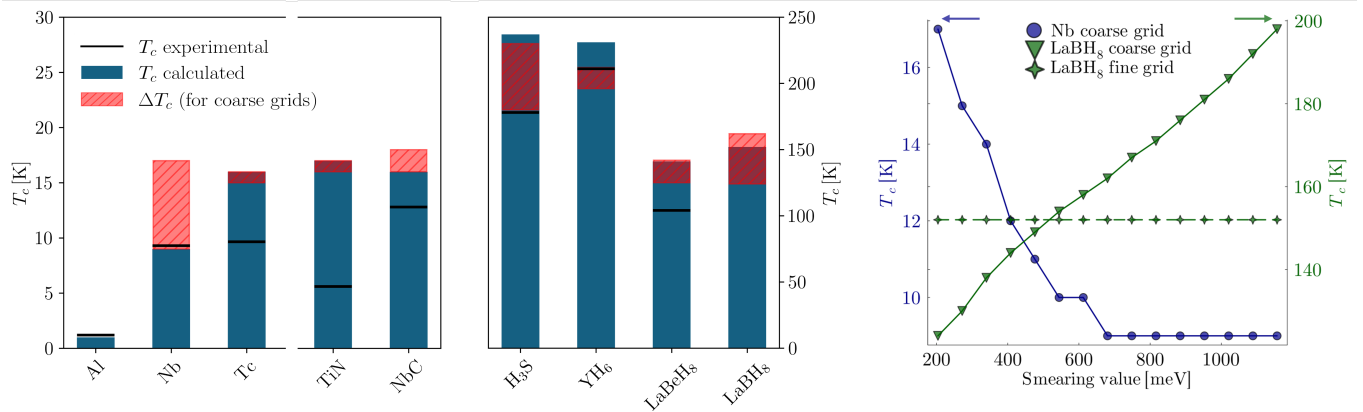


Figure 4: Comparison of T_c values for different smearing values for materials in the benchmark study. Left: The calculated T_c 's with $cDOS+\mu$ are shown as blue bars, the experimental values as black lines. For LaBH₈, no experimental data is available. Red and crosshatched bars indicate the T_c values in the unconverged region. Right: Convergence behavior of Nb (blue dots) and LaBH₈ (green triangles and stars) with respect to smearing. The lines serve as guides to the eye.

in Chevrel phases, multigap superconductors, or low dimensional systems [31].

IsoME was designed as a robust and user-friendly framework for calculating superconducting properties. Nevertheless, for reliable T_c predictions and proper interpretation of the results, several aspects must be considered when using IsoME:

First, accurate results can only be achieved through carefully conducted convergence tests for the input files. In particular, the $\alpha^2F(\omega)$ data needs to be of sufficient quality. In the following, we examine how different Brillouin zone grids influence T_c . The electron-phonon coupling for most materials in Tab. II was computed with QUANTUM ESPRESSO, where very dense q -grids can get prohibitively expensive, requiring smearing techniques to facilitate convergence. However, as Fig. 4 illustrates, varying the smearing parameters in the $\alpha^2F(\omega)$ calculations can lead to significant deviations in the predicted T_c . In several instances (e.g., H₃S, YH₆, LaBeH₈, and LaBH₈), convergence could not be attained with the QUANTUM ESPRESSO $\alpha^2F(\omega)$ data. To overcome this limitation, we interpolated the data to a significantly denser grid using EPW, effectively eliminating the dependence on smearing. The right panel of Fig. 4 further illustrates this behavior: while Nb attains convergence even with coarser grids for larger smearing values, LaBH₈ fails to converge under these conditions. Although these results were obtained using the $cDOS+\mu$ approximation, we observed a consistent trend across different theoretical approaches.

Second, the choice of μ significantly influences the results. Traditionally, μ^* is treated as an adjustable parameter and is typically chosen within the range of 0.1 to 0.16 to fit experimental values. For fully *ab-initio* calculations, μ must be computed and μ_E^* adapted according to Eq. (2), as was done for the results presented in Tab. II.

In light of these considerations, we compare the results presented in Tab. II with those available in the literature and reexamine YH₆ and H₃S, which were also studied by some of the present authors in Ref. [27]. First, a comment on the semi-

empirical approximations: In the present work, the McMillan formula modified by Allen-Dynes was applied, whereas in Ref. [27], the original McMillan equation as given in Eq. (14) in the SM [36] was used together with a μ_{AD}^* of 0.1. If we employ the McMillan equation and the same μ_{AD}^* for YH₆ and H₃S, we obtain the previously reported T_c 's of 154 and 173 K, respectively. Additionally, also T_c^{ML} is reproduced when setting $\mu_{AD}^* = 0.1$. Second, comparing T_c 's based on ME theory is less straightforward. While our results are based on the isotropic approximation, the findings in Ref. [27] are obtained from anisotropic calculations. To ensure a meaningful comparison, we performed IsoME calculations using the same parameters as reported in Ref. [27], including a Matsubara frequency cutoff ω_c of 6,000 meV, an electronic energy cutoff of 1,000 meV, and an unmodified μ_E^* . Under these conditions, our results across all approximations deviate by no more than 7% for YH₆ and 5% for H₃S.

CONCLUSION

We have developed the open-source Julia package IsoME, which provides a straightforward and efficient method for solving the isotropic Migdal-Eliashberg equations and evaluating T_c across different levels of approximation. These range from the semi-empirical McMillan Allen Dynes formula and the ML variant to the isotropic Migdal-Eliashberg approach, which can include either a constant or variable DOS and static Coulomb interactions. To demonstrate the accuracy and versatility of the code, we conducted a benchmark study on a diverse set of materials, including elementary, binary alloy, and ternary hydride superconductors, and compared the results to existing literature. Although the constant DOS approximation works well for many conventional superconductors, IsoME's flexible framework also supports the analysis of systems with complex electronic structures, which require both a refined treatment of the DOS near the Fermi level and the explicit inclusion of Coulomb interactions.

IsoME represents a significant advancement in the computational treatment of superconductivity, by offering multiple levels of approximation and a dedicated T_c search mode. This makes it a valuable tool for both theoretical investigations and high-throughput material discovery, paving the way for more accurate and efficient predictions of superconducting properties.

II. METHODS

Isotropic Migdal-Eliashberg theory

Conventional superconductivity arises from the formation of Cooper pairs, where an attractive interaction between electrons mediated by the electron-phonon coupling enables them to overcome the repulsive Coulomb interaction. This is described by ME theory, most conveniently formulated within the Nambu-Gor'kov formalism [33], leading to a generalized 2×2 Green's function propagator in Matsubara frequency space given by

$$\hat{G}_{nk}(i\omega_j) = \begin{pmatrix} G_{nk}(i\omega_j) & F_{nk}(i\omega_j) \\ F_{nk}^*(i\omega_j) & -G_{n-\mathbf{k}}(-i\omega_j) \end{pmatrix}. \quad (3)$$

The diagonal elements describe single particle excitations, the off-diagonal elements are the anomalous propagators describing the Cooper-pair amplitude, with band index n , wavevector \mathbf{k} , and $i\omega_j$ as fermionic Matsubara frequencies. The Dyson equation relates the interacting (G_{nk}) and non-interacting Green's functions (G_{nk}^0) via a self-energy $\hat{\Sigma}_{nk}(i\omega_j)$ [62, 63]

$$\hat{G}_{nk}^{-1}(i\omega_j) = \hat{G}_{nk}^{0-1}(i\omega_j) - \hat{\Sigma}_{nk}(i\omega_j), \quad (4)$$

which can be further decomposed in Nambu space using the Pauli matrices τ_i [64]:

$$\hat{\Sigma}_{nk}(i\omega_j) = i\omega_j [1 - Z_{nk}(i\omega_j)] \hat{\tau}_0 + \chi_{nk}(i\omega_j) \hat{\tau}_3 + \phi_{nk}(i\omega_j) \hat{\tau}_1. \quad (5)$$

The as of yet unknown components of the self-energy can be identified as the mass renormalization function Z , the energy shift χ , and the anomalous self-energy ϕ [27].

On the other hand, based on the Fröhlich Hamiltonian for a coupled electron-phonon system with Coulomb interactions and employing Migdal's approximation [3, 4, 65], we can find an alternative expression for the electron self-energy $\hat{\Sigma}_{nk}(i\omega_n)$ given by

$$\hat{\Sigma}_{nk}(i\omega_j) = -\frac{1}{\beta} \sum_{\mathbf{k}'n'j'} \hat{\tau}_3 \hat{G}_{n'\mathbf{k}'}(i\omega_{j'}) \left[W_{n\mathbf{k},n'\mathbf{k}'}(i\omega_j - i\omega_{j'}) + \sum_{\lambda} |g_{n'\lambda}(\mathbf{k}, \mathbf{k}')|^2 D_{\mathbf{k}-\mathbf{k}'\lambda}(i\omega_j - i\omega_{j'}) \right]. \quad (6)$$

Here, the first term describes the dynamically screened vertex-corrected Coulomb electron-electron interaction $W_{n\mathbf{k},n'\mathbf{k}'}(i\omega_j - i\omega_{j'})$, while the second term describes the interaction of electrons and phonons (with mode index λ)

via the electron-phonon coupling matrix element $g_{n'\lambda}(\mathbf{k}, \mathbf{k}')$ and the phonon propagator $D_{\mathbf{k}-\mathbf{k}'\lambda}(i\omega_n - i\omega_{j'})$ [65, 66]. The inverse temperature is denoted by $\beta = (k_B T)^{-1}$.

Assuming a static Coulomb interaction [32] and using the spectral representation of $D_{\mathbf{k}-\mathbf{k}'\lambda}(i\omega_n - i\omega_{j'})$, the electron self-energy from Eq. (6) becomes

$$\hat{\Sigma}_{nk}(i\omega_j) = -\frac{1}{\beta} \sum_{\mathbf{k}'n'j'} \hat{\tau}_3 \hat{G}_{n'\mathbf{k}'}(i\omega_{j'}) \hat{\tau}_3 \times \left[W_{n\mathbf{k},n'\mathbf{k}'} - \int_0^\infty d\omega \frac{\alpha^2 F_{n\mathbf{k},n'\mathbf{k}'}(\omega)}{N(\varepsilon_F)} \frac{2\omega}{(\omega_j - \omega_{j'})^2 + \omega^2} \right], \quad (7)$$

where we have introduced the Eliashberg spectral function [65, 66]

$$\alpha^2 F_{n\mathbf{k},n'\mathbf{k}'}(\omega) = N(\varepsilon_F) \sum_{\lambda} |g_{n'\lambda}(\mathbf{k}, \mathbf{k}')|^2 B_{\mathbf{k}-\mathbf{k}'\lambda}(\omega), \quad (8)$$

and the density of states per spin at the Fermi level ε_F , $N(\varepsilon_F)$. Note: In most cases, the fully interacting phonon Green's function is well approximated by choosing $B_{\mathbf{k}-\mathbf{k}'\lambda}(\omega) \approx \delta(\omega - \omega_{\mathbf{k}-\mathbf{k}'\lambda})$ [65].

Lastly, defining the electron-phonon coupling parameter as [6, 67]

$$\lambda_{n\mathbf{k},n'\mathbf{k}'}(\omega_j) = \int_0^\infty d\omega \alpha^2 F_{n\mathbf{k},n'\mathbf{k}'}(\omega) \frac{2\omega}{\omega_j^2 + \omega^2} \quad (9)$$

allows us to rewrite Eq. (7) in a more compact form

$$\hat{\Sigma}_{nk}(i\omega_j) = -\frac{1}{\beta} \sum_{\mathbf{k}'n'j'} \hat{\tau}_3 \hat{G}_{n'\mathbf{k}'}(i\omega_{j'}) \hat{\tau}_3 \times \left[W_{n\mathbf{k},n'\mathbf{k}'} - \frac{\lambda_{n\mathbf{k},n'\mathbf{k}'}(\omega_j - \omega_{j'})}{N(\varepsilon_F)} \right]. \quad (10)$$

By comparing the two different expressions for the self-energy in Eq. (5) and Eq. (10), we arrive at a set of coupled equations - the *anisotropic full-bandwidth Migdal-Eliashberg equations* - that determine the previously introduced functions Z , χ and ϕ , as discussed in [Eqs. (13)-(16)] of Ref. [27] and allow a very detailed, wave-vector resolved investigation of the properties of the superconducting phase.

Solving these equations is extremely demanding computationally, as the electron-phonon coupling can vary significantly near the Fermi surface, requiring very fine \mathbf{k} -point sampling. However, for most materials - except for a few notable layered systems such as MgB_2 [68–70], CaC_6 [71, 72], and NbS_2 [73] - this complexity can be mitigated by employing the isotropic approximation, where all quantities are averaged over the Brillouin zone [32, 74].

In particular, for the Eliashberg spectral function and the static Coulomb interaction we get

$$\alpha^2 F(\omega) = \frac{1}{N(\varepsilon_F)^2} \sum_{n\mathbf{k},n'\mathbf{k}'} \alpha^2 F_{n\mathbf{k},n'\mathbf{k}'}(\omega) \delta(\varepsilon_{n\mathbf{k}} - \varepsilon_F) \delta(\varepsilon_{n'\mathbf{k}'} - \varepsilon_F) \quad (11)$$

$$W(\varepsilon, \varepsilon') = \frac{1}{N(\varepsilon)N(\varepsilon')} \sum_{n\mathbf{k}, n'\mathbf{k}'} W_{n\mathbf{k}, n'\mathbf{k}'} \delta(\varepsilon_{n\mathbf{k}} - \varepsilon) \delta(\varepsilon_{n'\mathbf{k}'} - \varepsilon), \quad (12)$$

respectively.

The final set of coupled equations for the self-energy components in the isotropic approximation, as implemented in IsoME, is given by

$$Z(i\omega_j) = 1 + \frac{k_B T}{N(\varepsilon_F)\omega_j} \int d\varepsilon' N(\varepsilon') \sum_j \frac{\omega_j Z(i\omega_j)}{\Theta(\varepsilon', i\omega_j)} \lambda(\omega_j - \omega_j) \quad (13a)$$

$$\chi(i\omega_j) = -\frac{k_B T}{N(\varepsilon_F)} \int d\varepsilon' N(\varepsilon') \sum_j \frac{\varepsilon' - \mu_F + \chi(i\omega_j)}{\Theta(\varepsilon', i\omega_j)} \lambda(\omega_j - \omega_j) \quad (13b)$$

$$\phi^{ph}(i\omega_j) = \frac{k_B T}{N(\varepsilon_F)} \int d\varepsilon' N(\varepsilon') \sum_j \frac{\phi(\varepsilon', i\omega_j)}{\Theta(\varepsilon', i\omega_j)} \lambda(\omega_j - \omega_j) \quad (13c)$$

$$\phi^c(\varepsilon) = -k_B T \int d\varepsilon' N(\varepsilon') W(\varepsilon, \varepsilon') \sum_j \frac{\phi(\varepsilon', i\omega_j)}{\Theta(\varepsilon', i\omega_j)} \quad (13d)$$

$$N_e = \int d\varepsilon' N(\varepsilon') \left[1 - 2k_B T \sum_j \frac{\varepsilon' - \mu_F + \chi(i\omega_j)}{\Theta(\varepsilon', i\omega_j)} \right], \quad (13e)$$

with $\Theta(\varepsilon, i\omega_j) = [\omega_j Z(i\omega_j)]^2 + [\varepsilon - \mu_F + \chi(i\omega_j)]^2 + [\phi(\varepsilon, i\omega_j)]^2$ and $\phi(\varepsilon, i\omega_j) = \phi^{ph}(\omega_j) + \phi^c(\varepsilon)$. A detailed derivation is not within the scope of this manuscript and can be found elsewhere [31, 41]. The last Eq. (13e) fixes the electron number and is used to determine the chemical potential μ_F self-consistently [27, 75]. From the anomalous self-energy ϕ and the renormalization function Z , the superconducting gap function can be obtained via

$$\Delta(\varepsilon, i\omega_j) = \frac{\phi(\varepsilon, i\omega_j)}{Z(i\omega_j)}. \quad (14)$$

The critical superconducting temperature T_c is defined as the temperature for which Δ vanishes.

Equation (14) concludes the theoretical framework. In the

following, we discuss numerical challenges and provide implementation details. In equations involving a sum over Matsubara frequencies, the summation formally extends over infinitely many frequencies. To perform such an infinite sum numerically, a cutoff frequency, ω_c , is introduced as a convergence parameter. λ decays as $1/\omega_j^2$ and thus Z , χ , and ϕ^{ph} decay as $1/\omega_j^4$, ensuring convergence for relatively small ω_c (of the order of 10-20 times the Debye frequency of the system). This is not the case for ϕ^c and N_e , where considerably higher cutoffs are needed. A similar argument holds for the integrals over real energies ε , where electron-phonon interactions are restricted to energies close to the Fermi energy while Coulomb interactions decay considerably slower. One can improve convergence and accuracy by approximating $Z(i\omega_j) = 1$, $\phi(\varepsilon, i\omega_j) = 0$ and $\chi(i\omega_j) = 0$ for $\omega_j > \omega_c$ and $|\varepsilon| > \varepsilon_c$, allowing to rewrite Eqs. (13d) and (13e) as [31, 76]

$$\phi^c(\varepsilon) = \int d\varepsilon' N(\varepsilon') W(\varepsilon, \varepsilon') \left\{ \frac{\phi^c(\varepsilon') \tanh \left[\frac{\beta}{2} \sqrt{(\varepsilon' - \mu_F)^2 + \phi^{c2}(\varepsilon')} \right]}{2 \sqrt{(\varepsilon' - \mu_F)^2 + \phi^{c2}(\varepsilon')}} + 2k_B T \sum_{j=0}^{\omega_j \leq \omega_c} \left[\frac{\phi(\varepsilon', i\omega_j)}{\Theta(\varepsilon', i\omega_j)} - \frac{\phi^c(\varepsilon')}{\omega_j^2 + (\varepsilon' - \mu_F)^2 + \phi^{c2}(\varepsilon')} \right] \right\} \quad (15a)$$

$$N_e \approx \int d\varepsilon N(\varepsilon) \left\{ 2n_F(\varepsilon - \mu_F) - 4k_B T \sum_{j=0}^{\omega_j \leq \omega_c} \left[\frac{\varepsilon - \mu_F + \chi(i\omega_j)}{\Theta(\varepsilon, i\omega_j)} - \frac{\varepsilon - \mu_F}{\omega_j^2 + (\varepsilon - \mu_F)^2} \right] \right\}. \quad (15b)$$

To maintain charge neutrality in vDOS+ μ and vDOS+W calculations, the chemical potential should be continuously updated according to Eq. (15b).

Within IsoME, we found that choosing $\omega_c \sim 5-10$ eV is sufficient to ensure both computational feasibility and high

accuracy. Additionally, we implemented a sparse-sampling scheme to enhance the efficiency of the summation over Matsubara frequencies [47–49]. Given that the overhead associated with setting up the irreducible sparse-sampling basis outweighs the time savings from the summation for temperatures

above 2 K, sparse-sampling is activated only for temperatures below this threshold.

III. COMPUTATIONAL DETAILS

DFT and DFPT calculations

Density functional (perturbation) theory calculations were performed using QUANTUM ESPRESSO [37–39], scalar-relativistic optimized norm-conserving Vanderbilt pseudopotentials [77], and the PBE-GGA exchange and correlation functional [78]. For the following materials, a plane-wave cutoff energy for the wavefunctions of 80 Ry was applied, and the respective \mathbf{k} -grid for each material is given in parenthesis: Nb (16³), Tc (18³), Sn (8×8×14), TiN (12³), NbC (14³), H₃S (20³), YH₆ (16³), and LaBeH₈ (12³). A cutoff of 50 Ry and a \mathbf{k} -grid of 20³ were used for Al. LaBH₈ was calculated with a cutoff of 90 Ry and a 16³ \mathbf{k} -grid. All materials were calculated with a Methfessel-Paxton [79] smearing of 0.02 Ry, except YH₆, where a smearing of 0.04 Ry was applied. For the relaxation of lattice parameters and atomic positions, the convergence threshold was set to 10⁻⁷ Ry and 10⁻⁶ Ry/a₀ for the total energy and the forces, respectively. DFPT calculations were conducted on a coarse 6³ \mathbf{q} -grid with a self-consistency threshold of 10⁻¹⁴ or lower for all materials. The fine grid consisted of 48³ \mathbf{k} - and \mathbf{q} -points for YH₆ and H₃S, and 30³ \mathbf{k} - and \mathbf{q} -points for LaBeH₈ and LaBH₈. More details on the interpolation to the fine grids are provided in [27, 34].

IsoME

For the calculations with IsoME, a Matsubara frequency cutoff ω_{cut} of 7,000 meV was employed. In variable DOS calculations, the chemical potential was consistently updated. The energy cutoff ω_{cut} for all quantities was set to 5,000 meV, except in the calculation for the energy shift and the μ update, where a reduced cutoff ω_{shiftcut} of 2,000 meV was applied.

In cases where both a DOS and a W file are supplied, we renormalize μ based on the $N(\varepsilon_F)$ from the DOS. This not only ensures internal consistency but also facilitates improved convergence of μ with respect to the Brillouin zone grid sampling in our GW computations. When calculating μ_E^* from a provided μ , the characteristic cutoff frequency for the phonon-introduced interaction ω_{ph} was set to the highest phonon frequency, while the characteristic electronic energy scale $\text{typ}E_I$ was defined by the width of the bands crossing the Fermi level.

Calculation of W

Based on the DFT calculations in the normal state, the static polarizability function can be computed by applying the ran-

dom phase approximation (RPA) as [42, 44]

$$\chi_{\mathbf{G}\mathbf{G}'}(\mathbf{q}, 0) = \frac{2}{N_{\mathbf{k}}} \sum_{n'}^{\text{occ.}} \sum_n^{\text{emp.}} \sum_{\mathbf{k}} \frac{\rho_{n\mathbf{k}, n'\mathbf{k}+\mathbf{q}}(\mathbf{G}) \left(\rho_{n\mathbf{k}, n'\mathbf{k}+\mathbf{q}}(\mathbf{G}') \right)^*}{\varepsilon_{n'\mathbf{k}+\mathbf{q}} - \varepsilon_{n\mathbf{k}}} \quad (16)$$

where $N_{\mathbf{k}}$ is the total number of wave vectors \mathbf{k} in the first Brillouin zone, \mathbf{G} is a reciprocal lattice vector, and

$$\rho_{n\mathbf{k}, n'\mathbf{k}+\mathbf{q}}(\mathbf{G}) = \int \psi_{n'\mathbf{k}+\mathbf{q}}^*(\mathbf{r}) e^{i(\mathbf{q}+\mathbf{G})\cdot\mathbf{r}} \psi_{n\mathbf{k}}(\mathbf{r}) d\mathbf{r} \quad (17)$$

denotes the plane-wave matrix element. The inverse static dielectric function is expressed in terms of the static polarizability function $\chi_{\mathbf{G}\mathbf{G}'}$:

$$\varepsilon_{\mathbf{G}\mathbf{G}'}^{-1}(\mathbf{q}, 0) = \delta_{\mathbf{G}\mathbf{G}'} - \frac{4\pi e^2}{\Omega} \frac{\chi_{\mathbf{G}\mathbf{G}'}(\mathbf{q}, 0)}{|\mathbf{q} + \mathbf{G}||\mathbf{q} + \mathbf{G}'|}. \quad (18)$$

Since the screened Coulomb interaction is written with the Fourier transformation of ε^{-1} as

$$W(\mathbf{r}, \mathbf{r}', 0) = \int d\mathbf{r}'' \frac{\varepsilon^{-1}(\mathbf{r}, \mathbf{r}'', 0)}{|\mathbf{r}'' - \mathbf{r}'|}, \quad (19)$$

the screened Coulomb matrix element describing the scattering between two Kohn-Sham states is given by

$$\begin{aligned} W_{n\mathbf{k}, n'\mathbf{k}+\mathbf{q}} &= \int \int \psi_{n'\mathbf{k}+\mathbf{q}}^*(\mathbf{r}) \psi_{n\mathbf{k}}(\mathbf{r}) W(\mathbf{r}, \mathbf{r}', 0) \\ &\quad \times \psi_{n'\mathbf{k}-\mathbf{q}}^*(\mathbf{r}') \psi_{n-\mathbf{k}}(\mathbf{r}') d\mathbf{r} d\mathbf{r}' \\ &= \frac{4\pi e^2}{N_{\mathbf{q}} \Omega} \sum_{\mathbf{G}, \mathbf{G}'} \varepsilon_{\mathbf{G}\mathbf{G}'}^{-1}(\mathbf{q}) \frac{\rho_{n\mathbf{k}, n'\mathbf{k}+\mathbf{q}}(\mathbf{G}) \left(\rho_{n\mathbf{k}, n'\mathbf{k}+\mathbf{q}}(\mathbf{G}') \right)^*}{|\mathbf{q} + \mathbf{G}||\mathbf{q} + \mathbf{G}'|}. \end{aligned} \quad (20)$$

Here, the relation $\psi_{n-\mathbf{k}}(\mathbf{r}) = \psi_{n\mathbf{k}}^*(\mathbf{r})$ is used, which holds if the Hamiltonian is invariant under time-reversal symmetry.

In this work, we used BerkeleyGW [42–44] to compute $\chi_{\mathbf{G}\mathbf{G}'}(\mathbf{q}, 0)$ and $\varepsilon_{\mathbf{G}\mathbf{G}'}^{-1}(\mathbf{q}, 0)$ as defined in Eqs. (16) and (18), respectively. These quantities were evaluated for \mathbf{G} and \mathbf{G}' satisfying $|\mathbf{G}^2| < |E_{\text{cut}}|$, where E_{cut} is the dielectric energy cutoff and was set to 25 Ry for all materials. An 8³ \mathbf{q} -grid was used for Nb, Al, and TiN; an 8 × 8 × 4 \mathbf{q} -grid for Tc; and a 6³ \mathbf{q} -grid for NbC, H₃S, YH₆, LaBeH₈, and LaBH₈. The energy-dependent Coulomb interaction $W(\varepsilon, \varepsilon')$ was computed using Eqs. (12) and (20).

ACKNOWLEDGMENTS

We thank P.N. Ferreira, F. Jöbstl, and M. Sahoo, for testing IsoME and providing feedback. The authors acknowledge P.N. Ferreira for contributing data on H₃S and YH₆, and D. Khodachenko for data on LaBeH₈ and LaBH₈. We are also very grateful to A. Sanna for many fruitful discussions and sharing data for W to compare and benchmark. R.L. acknowledges the Carl Tryggers Stiftelse för Vetenskaplig Forskning (CTS 23: 2934). H.M. and E.R.M. acknowledge the support from the U.S. National Science Foundation under Grant No.

OAC-2103991. Z.Z. and Z.L. acknowledge the support from the U.S. National Science Foundation under Grant No. DMR-2440763. Superconductivity computations were performed on local workstations and the ICluster at TU Graz. Calculations of the Coulomb interaction were performed on the Frontera supercomputer at the Texas Advanced Computing Center via the Leadership Resource Allocation No. DMR22004 and DMR22042.

DECLARATION OF COMPETING INTEREST

The authors declare that they have no known competing financial interests or personal relationships that could have appeared to influence the work reported in this paper.

CODE AVAILABILITY

IsoME is available as a registered Julia package (juliahub.com/ui/Packages/General/IsoME), on GitHub (github.com/cheil/IsoME.jl), and Zenodo (DOI:10.5281/zenodo.14967551).

DATA AVAILABILITY

Data is made available with the code. Any additional data will be made available upon request.

AUTHOR CONTRIBUTIONS

E.K. and D.S. contributed equally. E.K., D.S., and C.H. developed the code and performed the superconductivity calculations, while R.L. derived the refined μ_F update procedure. H.M. and Z.Z. carried out the *GW* calculations of the Coulomb interaction. C.H. conceived and supervised the project, with R.M. and Z.L. providing additional oversight. All authors contributed to discussions and revised the manuscript.

DECLARATION OF GENERATIVE AI AND AI-ASSISTED TECHNOLOGIES IN THE WRITING PROCESS

In preparing this paper, the authors used ChatGPT to help improve readability and language. After using this tool, the authors reviewed and edited the content as needed and take full responsibility for the content of the published article.

-
- [1] H. Onnes, *Comm. Phys. Lab. Univ. Leiden*, 122 (1911).
- [2] J. Bardeen, L. N. Cooper, and J. R. Schrieffer, *Phys. Rev.* **108**, 1175 (1957).
- [3] A. B. Migdal, *Zhur. Eksptl'. i Teoret. Fiz.* **Vol: 34**, (1958).
- [4] G. M. Eliashberg, *Sov. Phys. - JETP (Engl. Transl.)*; (United States) **11:3**, (1960).
- [5] W. L. McMillan, *Phys. Rev.* **167**, 331 (1968).
- [6] P. B. Allen and R. C. Dynes, *Phys. Rev. B* **12**, 905 (1975).
- [7] A. Simon, R. Foster, M. Sahoo, J. Shi, E. Batson, F. Incalza, C. Heil, and K. K. Berggren, *Ab initio modeling of single-photon detection in superconducting nanowires* (2025), [arXiv:2501.13791 \[cond-mat.supr-con\]](https://arxiv.org/abs/2501.13791).
- [8] R. Setzu, E. Baggetta, and J. C. Villégier, *Journal of Physics: Conference Series* **97**, 012077 (2008).
- [9] Y. Nakamura, H. Terai, K. Inomata, T. Yamamoto, W. Qiu, and Z. Wang, *Applied Physics Letters* **99**, 212502 (2011), https://pubs.aip.org/aip/apl/article-pdf/doi/10.1063/1.3663539/14460294/212502_1_online.pdf.
- [10] L. N. Oliveira, E. K. U. Gross, and W. Kohn, *Phys. Rev. Lett.* **60**, 2430 (1988).
- [11] M. Lüders, M. A. L. Marques, N. N. Lathiotakis, A. Floris, G. Profeta, L. Fast, A. Continenza, S. Massidda, and E. K. U. Gross, *Phys. Rev. B* **72**, 024545 (2005).
- [12] M. A. L. Marques, M. Lüders, N. N. Lathiotakis, G. Profeta, A. Floris, L. Fast, A. Continenza, E. K. U. Gross, and S. Massidda, *Phys. Rev. B* **72**, 024546 (2005).
- [13] B. Lilia, R. Hennig, P. Hirschfeld, G. Profeta, A. Sanna, E. Zurek, W. E. Pickett, M. Amsler, R. Dias, M. I. Eremets, *et al.*, *Journal of Physics: Condensed Matter* **34**, 183002 (2022).
- [14] C. J. Pickard, I. Errea, and M. I. Eremets, *Annual Review of Condensed Matter Physics* **11**, 57 (2020).
- [15] J. Flores-Livas, L. Boeri, A. Sanna, G. Profeta, R. Arita, and M. Eremets, *Physics Reports* **856** (2020).
- [16] G. S. Boebinger, A. V. Chubukov, I. R. Fisher, F. M. Grosche, P. J. Hirschfeld, S. R. Julian, B. Keimer, S. A. Kivelson, A. P. Mackenzie, Y. Maeno, *et al.*, *arXiv preprint arXiv:2411.10522* (2024).
- [17] D. Duan, Y. Liu, F. Tian, D. Li, X. Huang, Z. Zhao, H. Yu, B. Liu, W. Tian, and T. Cui, *Scientific Reports* **4**, 6968 (2014), publisher: Nature Publishing Group.
- [18] A. P. Drozdov, M. I. Eremets, I. A. Troyan, V. Ksenofontov, and S. I. Shylin, *Nature* **525**, 73 (2015), publisher: Nature Publishing Group.
- [19] H. Liu, I. I. Naumov, R. Hoffmann, N. W. Ashcroft, and R. J. Hemley, *Proceedings of the National Academy of Sciences* **114**, 6990 (2017), <https://www.pnas.org/doi/pdf/10.1073/pnas.1704505114>.
- [20] M. Somayazulu, M. Ahart, A. K. Mishra, Z. M. Geballe, M. Baldini, Y. Meng, V. V. Struzhkin, and R. J. Hemley, *Phys. Rev. Lett.* **122**, 027001 (2019).
- [21] I. A. Troyan, D. V. Semenok, A. G. Kvashnin, A. V. Sadakov, O. A. Sobolevskiy, V. M. Pudalov, A. G. Ivanova, V. B. Prakapenka, E. Greenberg, A. G. Gavriluk, I. S. Lyubutin, V. V. Struzhkin, A. Bergara, I. Errea, R. Bianco, M. Calandra, F. Mauri, L. Monacelli, R. Akashi, and A. R. Oganov, *Advanced Materials* **33**, 2006832 (2021),

- <https://onlinelibrary.wiley.com/doi/pdf/10.1002/adma.202006832>.
- [22] Y. Song, J. Bi, Y. Nakamoto, K. Shimizu, H. Liu, B. Zou, G. Liu, H. Wang, and Y. Ma, *Phys. Rev. Lett.* **130**, 266001 (2023).
- [23] S. Di Cataldo, C. Heil, W. von der Linden, and L. Boeri, *Phys. Rev. B* **104**, L020511 (2021).
- [24] Z. Zhang, T. Cui, M. J. Hutcheon, A. M. Shipley, H. Song, M. Du, V. Z. Kresin, D. Duan, C. J. Pickard, and Y. Yao, *Physical Review Letters* **128**, 047001 (2022).
- [25] J. Bezanson, A. Edelman, S. Karpinski, and V. B. Shah, *SIAM Review* **59**, 65 (2017), <https://doi.org/10.1137/141000671>.
- [26] (), the IsoME code can be obtained via github at [...] or directly as a Julia package.
- [27] R. Lucrezi, P. P. Ferreira, S. Hajinazar, H. Mori, H. Paudyal, E. R. Margine, and C. Heil, *Communications Physics* **7**, 1 (2024), publisher: Nature Publishing Group.
- [28] W. Sano, T. Koretsune, T. Tadano, R. Akashi, and R. Arita, *Phys. Rev. B* **93**, 094525 (2016).
- [29] A. Sanna, J. A. Flores-Livas, A. Davydov, G. Profeta, K. Dewhurst, S. Sharma, and E. K. U. Gross, *Journal of the Physical Society of Japan* **87**, 041012 (2018), <https://doi.org/10.7566/JPSJ.87.041012>.
- [30] T. Wang, T. Nomoto, Y. Nomura, H. Shinaoka, J. Otsuki, T. Koretsune, and R. Arita, *Phys. Rev. B* **102**, 134503 (2020).
- [31] C. Pellegrini, R. Heid, and A. Sanna, *Journal of Physics: Materials* **5**, 024007 (2022), publisher: IOP Publishing.
- [32] C. Pellegrini and A. Sanna, *Nature Reviews Physics* **6** (2024).
- [33] Y. Nambu, *Phys. Rev.* **117**, 648 (1960).
- [34] D. Khodachenko, R. Lucrezi, P. Ferreira, M. Aichhorn, and C. Heil, *Computational Materials Today* **4**, 100015 (2024).
- [35] P. Morel and P. W. Anderson, *Phys. Rev.* **125**, 1263 (1962).
- [36] The Supplementary Material is available at [...].
- [37] P. Giannozzi, S. Baroni, N. Bonini, M. Calandra, R. Car, C. Cavazzoni, D. Ceresoli, G. L. Chiarotti, M. Cococcioni, I. Dabo, A. Dal Corso, S. de Gironcoli, S. Fabris, G. Fratesi, R. Gebauer, U. Gerstmann, C. Gougoussis, A. Kokalj, M. Lazzeri, L. Martin-Samos, N. Marzari, F. Mauri, R. Mazzarello, S. Paolini, A. Pasquarello, L. Paulatto, C. Sbraccia, S. Scandolo, G. Sclauzero, A. P. Seitsonen, A. Smogunov, P. Umari, and R. M. Wentzcovitch, *Journal of Physics: Condensed Matter* **21**, 395502 (19pp) (2009).
- [38] P. Giannozzi, O. Andreussi, T. Brumme, O. Bunau, M. B. Nardelli, M. Calandra, R. Car, C. Cavazzoni, D. Ceresoli, M. Cococcioni, N. Colonna, I. Carnimeo, A. D. Corso, S. de Gironcoli, P. Delugas, R. A. D. Jr, A. Ferretti, A. Floris, G. Fratesi, G. Fugallo, R. Gebauer, U. Gerstmann, F. Giustino, T. Gorni, J. Jia, M. Kawamura, H.-Y. Ko, A. Kokalj, E. Küçükbenli, M. Lazzeri, M. Marsili, N. Marzari, F. Mauri, N. L. Nguyen, H.-V. Nguyen, A. O. de-la Roza, L. Paulatto, S. Poncé, D. Rocca, R. Sabatini, B. Santra, M. Schlipf, A. P. Seitsonen, A. Smogunov, I. Timrov, T. Thonhauser, P. Umari, N. Vast, X. Wu, and S. Baroni, *Journal of Physics: Condensed Matter* **29**, 465901 (2017).
- [39] P. Giannozzi, O. Baseggio, P. Bonfà, D. Brunato, R. Car, I. Carnimeo, C. Cavazzoni, S. de Gironcoli, P. Delugas, F. Ferrari Ruffino, A. Ferretti, N. Marzari, I. Timrov, A. Urru, and S. Baroni, *The Journal of Chemical Physics* **152**, 154105 (2020), <https://doi.org/10.1063/5.0005082>.
- [40] E. R. Margine and F. Giustino, *Phys. Rev. B* **87**, 024505 (2013).
- [41] H. Lee, S. Poncé, K. Bushick, S. Hajinazar, J. Lafuente-Bartolome, J. Leveillee, C. Lian, J.-M. Lihm, F. Macheda, H. Mori, H. Paudyal, W. H. Sio, S. Tiwari, M. Zacharias, X. Zhang, N. Bonini, E. Kioupakis, E. R. Margine, and F. Giustino, *npj Computational Materials* **9**, 10.1038/s41524-023-01107-3 (2023).
- [42] M. S. Hybertsen and S. G. Louie, *Phys. Rev. B* **34**, 5390 (1986).
- [43] M. Rohlffing and S. G. Louie, *Phys. Rev. B* **62**, 4927 (2000).
- [44] J. Deslippe, G. Samsonidze, D. A. Strubbe, M. Jain, M. L. Cohen, and S. G. Louie, *Computer Physics Communications* **183**, 1269 (2012).
- [45] R. C. Dynes, *Solid State Communications* **10**, 615 (1972).
- [46] S. R. Xie, Y. Quan, A. C. Hire, B. Deng, J. M. DeStefano, I. Salinas, U. S. Shah, L. Fanfarillo, J. Lim, J. Kim, G. R. Stewart, J. J. Hamlin, P. J. Hirschfeld, and R. G. Hennig, *npj Computational Materials* **8**, 14 (2022).
- [47] H. Shinaoka, J. Otsuki, M. Ohzeki, and K. Yoshimi, *Physical Review B* **96**, 035147 (2017).
- [48] J. Li, M. Wallerberger, N. Chikano, C.-N. Yeh, E. Gull, and H. Shinaoka, *Physical Review B* **101**, 035144 (2020).
- [49] M. Wallerberger, S. Badr, S. Hoshino, S. Huber, F. Kakizawa, T. Koretsune, Y. Nagai, K. Nogaki, T. Nomoto, H. Mori, J. Otsuki, S. Ozaki, T. Plaikner, R. Sakurai, C. Vogel, N. Witt, K. Yoshimi, and H. Shinaoka, *SoftwareX* **21**, 101266 (2023).
- [50] B. T. Matthias, T. H. Geballe, and V. B. Compton, *Rev. Mod. Phys.* **35**, 1 (1963).
- [51] A. L. Giorgi, E. G. Szklarz, E. K. Storms, A. L. Bowman, and B. T. Matthias, *Phys. Rev.* **125**, 837 (1962).
- [52] P. Kong, V. S. Minkov, M. A. Kuzovnikov, A. P. Drozdov, S. P. Besedin, S. Mozaffari, L. Balicas, F. F. Balakirev, V. B. Prakapenka, S. Chariton, *et al.*, *Nature communications* **12**, 5075 (2021).
- [53] Y. Song, J. Bi, Y. Nakamoto, K. Shimizu, H. Liu, B. Zou, G. Liu, H. Wang, and Y. Ma, *Phys. Rev. Lett.* **130**, 266001 (2023).
- [54] M. Kawamura, Y. Hizume, and T. Ozaki, *Physical Review B* **101**, 134511 (2020).
- [55] A. Cucciarri, D. Naddeo, S. Di Cataldo, and L. Boeri, *Phys. Rev. B* **110**, L140502 (2024).
- [56] P. Ferreira, R. Lucrezi, I. Guilhon, M. Marques, L. Teles, C. Heil, and L. Eleno, *Materials Today Physics* **48**, 101547 (2024).
- [57] N. W. Ashcroft, *Phys. Rev. Lett.* **21**, 1748 (1968).
- [58] I. Errea, M. Calandra, C. J. Pickard, J. Nelson, R. J. Needs, Y. Li, H. Liu, Y. Zhang, Y. Ma, and F. Mauri, *Phys. Rev. Lett.* **114**, 157004 (2015).
- [59] I. Errea, F. Belli, L. Monacelli, A. Sanna, T. Koretsune, T. Tadano, R. Bianco, M. Calandra, R. Arita, F. Mauri, and J. A. Flores-Livas, *Nature* **578**, 66–69 (2020).
- [60] R. Lucrezi, E. Kogler, S. Cataldo, M. Aichhorn, L. Boeri, and C. Heil, *Communications Physics* **6**, 298 (2023).
- [61] R. Lucrezi, P. Nunes Ferreira, M. Aichhorn, and C. Heil, *Nature Communications* **15** (2024).
- [62] S. Poncé, E. Margine, C. Verdi, and F. Giustino, *Computer Physics Communications* **209**, 116–133 (2016).
- [63] R. D. Mattuck, *A guide to Feynman diagrams in the many-body problem*, 2nd ed., Dover books on physics and chemistry (Dover Publications, New York, 1992).
- [64] D. J. Scalapino, J. R. Schrieffer, and J. W. Wilkins, *Phys. Rev.* **148**, 263 (1966).
- [65] P. B. Allen and B. Mitrović, in *Solid State Physics*, Solid State Physics, Vol. 37, edited by H. Ehrenreich, F. Seitz, and D. Turnbull (Academic Press, 1983) pp. 1–92.
- [66] F. Marsiglio and J. P. Carbotte, *Electron - phonon superconductivity* (2001), [arXiv:cond-mat/0106143](https://arxiv.org/abs/cond-mat/0106143) [cond-mat.supr-con].
- [67] W. E. Pickett, *Physical Review B* **26**, 1186 (1982), publisher: American Physical Society.
- [68] J. Kortus, I. I. Mazin, K. D. Belashchenko, V. P. Antropov, and L. L. Boyer, *Phys. Rev. Lett.* **86**, 4656 (2001).

- [69] H. Choi, D. Roundy, H. Sun, M. Cohen, and S. Louie, *Nature* **418**, 758 (2002).
- [70] H. Choi, M. Cohen, and S. Louie, *Physica C: Superconductivity and its applications* **385**, 66 (2003).
- [71] R. S. Gonnelli, D. Daghero, D. Delaude, M. Tortello, G. A. Ummarino, V. A. Stepanov, J. S. Kim, R. K. Kremer, A. Sanna, G. Profeta, and S. Massidda, *Phys. Rev. Lett.* **100**, 207004 (2008).
- [72] A. Sanna, G. Profeta, A. Floris, A. Marini, E. K. U. Gross, and S. Massidda, *Phys. Rev. B* **75**, 020511 (2007).
- [73] C. Heil, S. Poncé, H. Lambert, M. Schlipf, E. R. Margine, and F. Giustino, *Phys. Rev. Lett.* **119**, 087003 (2017).
- [74] A. Davydov, A. Sanna, C. Pellegrini, J. K. Dewhurst, S. Sharma, and E. K. U. Gross, *Phys. Rev. B* **102**, 214508 (2020).
- [75] G. A. Ummarino, in *Emergent phenomena in correlated matter*, Band 3, edited by E. Pavarini, E. Koch, and U. Schollwöck (Forschungszentrum Jülich GmbH, Jülich, 2013).
- [76] (), a detailed derivation can be found in section Sxx of the Supplemental Material [36].
- [77] D. R. Hamann, *Phys. Rev. B* **88**, 085117 (2013).
- [78] J. P. Perdew, K. Burke, and M. Ernzerhof, *Phys. Rev. Lett.* **77**, 3865 (1996).
- [79] M. Methfessel and A. T. Paxton, *Phys. Rev. B* **40**, 3616 (1989).

Supplemental Material
for
IsoME: Streamlining High-Precision Eliashberg Calculations

Eva Kogler,¹ Dominik Spath,¹ Roman Lucrezi,^{1,2} Hitoshi Mori,³
Zien Zhu,⁴ Zhenglu Li,⁴ Elena R. Margine,³ and Christoph Heil^{1,†}

¹*Institute of Theoretical and Computational Physics,
Graz University of Technology, NAWI Graz, 8010, Graz, Austria*

²*Department of Materials and Environmental Chemistry,
Stockholm University, SE-10691 Stockholm, Sweden*

³*Department of Physics, Applied Physics,
and Astronomy, Binghamton University-SUNY,
Binghamton, New York 13902, USA*

⁴*Mork Family Department of Chemical Engineering and Materials Science,
University of Southern California, Los Angeles, California 90089, USA*

(Dated: March 5, 2025)

I. USAGE OF ISOME

ISOME [1] is a registered Julia package available for installation through various channels. To install ISOME using the Julia package manager, follow these steps:

1. Ensure that you have Julia 1.10 or later installed.
2. Open the Julia REPL and run:
 - `using Pkg`
 - `Pkg.add("IsoME")`

Alternatively, the package can also be obtained from GitHub or Zenodo [1]. Detailed usage instructions and further information are provided in the package documentation.

II. BENCHMARK AND CONVERGENCE TESTS

For comparison, Tab. I provides the T_c values for materials of our benchmark study, calculated with the default value of $\mu_{AD}^* = 0.12$. Additionally, when available, the results of SCDFT calculation from the literature are included.

TABLE I: Comparison of resulting T_c for different levels of theory within ISOME. T_c^{AD} , T_c^{ML} , $T_c^{E, \text{cdos}, \mu}$, $T_c^{E, \text{vdos}, \mu}$, T_c^{exp} , and T_c^{SCDFT} are the critical superconducting temperatures within McMillan Allen Dynes, the machine learned improvement of it, Migdal-Eliashberg constant DOS and variable DOS using $\mu_{AD}^* = 0.12$, Migdal-Eliashberg variable DOS, the experimental value, and the result obtained from SCDFT, respectively.

Compound	T_c^{AD} (K)	T_c^{ML} (K)	$T_c^{E, \text{cdos}, \mu}$ (K)	$T_c^{E, \text{vdos}, \mu}$ (K)	T_c^{exp} (K)	T_c^{SCDFT} (K)
Nb	9	9	9	8	9.1-9.5 [2]	11 [3]
Al	1.0	1.0	0.5	0.5	1.2 [2]	2 [3]
Tc	15	14	14	14	8.2-9.3-11.1 [2]	-
β -Sn	6	6	5	5	3.7 [2]	5 [3]
Pb (wSOC)	7	7	7	-	7.2 [2]	6 [3]
Pb (woSOC)	8	9	8	-	7.2 [2]	6 [3]
NbC	14	14	13	13	12.8* [4]	-
TiN	13	12	12	12	5.6* [2]	-
Nb ₂ S (225 GPa)	18	23	19	-	-	-
H ₃ S (200 GPa)	228	258	240	221	172-184 [5]	131 [6]
YH ₆ (200 GPa)	201	229	224	221	208-214 [7]	-
LaBeH ₈ (100 GPa)	120	127	130	131	104 [8]	-
LaBH ₈ (50 GPa)	133	145	138	142	-	-
BaSiH ₈ (30 GPa)	55	59	58	60	-	-

[†] Corresponding author: christoph.heil@tugraz.at

III. EQUATIONS

Starting from the most general form of the isotropic Eliashberg equations with static Coulomb interactions [Eq. (13a)-(13d) and Eq. (13e) in the main text], three simpler approximations can be derived, which are also implemented within IsoME. The abbreviations are discussed in Sec. II of the main text.

A. cDOS W

By assuming a constant DOS around the Fermi energy, the energy shift $\chi(\omega_j)$ vanishes, and the particle number equation is automatically satisfied. The remaining equations then simplify to

$$Z(i\omega_j) = 1 + \frac{\pi}{\beta\omega_j} \sum_{j'=0}^{\infty} \frac{\omega_{j'} Z(i\omega_{j'}) \lambda_{jj'}^{(-)}}{\sqrt{\Theta(0, \omega_{j'})}} \quad (1)$$

$$\phi^{ph}(i\omega_j) = \frac{\pi}{\beta} \sum_{j'=0}^{\infty} \frac{\phi(0, \omega_{j'}) \lambda_{jj'}^{(+)}}{\sqrt{\Theta(0, \omega_{j'})}} \quad (2)$$

$$\begin{aligned} \phi^c(\varepsilon) = & - \int d\varepsilon' W(\varepsilon, \varepsilon') N(\varepsilon') \left\{ \frac{\phi^c(\varepsilon') \tanh \left[\frac{\beta}{2} \sqrt{\varepsilon' + \phi^c(\varepsilon')} \right]}{2 \sqrt{\varepsilon'^2 + \phi^c(\varepsilon')}} \right. \\ & \left. + 2k_B T \sum_{n'=0}^M \left[\frac{\phi^{ph}(i\omega_{j'}) + \phi^c(\varepsilon')}{\Theta(\varepsilon', i\omega_{j'})} - \frac{\phi^c(\varepsilon')}{\omega_{j'}^2 + \varepsilon'^2 + \phi^c(\varepsilon')} \right] \right\} \quad (3) \end{aligned}$$

$$\phi(\varepsilon, i\omega_j) = \phi^{ph}(i\omega_j) + \phi^c(\varepsilon) \quad (4)$$

$$\Theta(\varepsilon, i\omega_j) = [\omega_j Z(i\omega_j)]^2 + \varepsilon^2 + \phi^2(\varepsilon, i\omega_j) \quad (5)$$

This is similar to the approach followed in Ref. [9].

B. vDOS μ^*

If the Coulomb repulsion between electrons varies slowly around the Fermi level, it can be approximated with a pseudopotential μ^* as demonstrated in Ref. [10]. The corresponding equations are given by

$$Z(i\omega_j) = 1 + \frac{k_B T}{N(\varepsilon_F) \omega_j} \int d\varepsilon N(\varepsilon) \sum_{j'=0}^{\infty} \frac{\omega_{j'} Z(i\omega_{j'}) \lambda_{jj'}^{(-)}}{\Theta(\varepsilon, i\omega_{j'})} \quad (6)$$

$$\chi(i\omega_j) = - \frac{k_B T}{N(\varepsilon_F)} \int d\varepsilon N(\varepsilon) \sum_{j'=0}^{\infty} \frac{\varepsilon - \mu_F + \chi(i\omega_{j'})}{\Theta(\varepsilon, i\omega_{j'})} \lambda_{jj'}^{(+)} \quad (7)$$

$$\phi(i\omega_j) = \frac{k_B T}{N(\varepsilon_F)} \int d\varepsilon N(\varepsilon) \sum_{j'=0}^{\infty} \frac{\phi(i\omega_{j'})}{\Theta(\varepsilon, i\omega_{j'})} [\lambda_{jj'}^{(+)} - 2\mu^*] \quad (8)$$

$$N_e = \int d\varepsilon N(\varepsilon) \left[1 - 2k_B T \sum_j \frac{\varepsilon - \mu_F + \chi(i\omega_j)}{\Theta(\varepsilon, i\omega_j)} \right] \quad (9)$$

$$\approx 2n_F(\varepsilon - \mu_F) - 4k_B T \sum_{j=0}^{\omega_j \leq \omega_c} \left[\frac{\varepsilon - \mu_F + \chi(i\omega_j)}{\Theta(\varepsilon, i\omega_j)} - \frac{\varepsilon - \mu_F}{\omega_j^2 + (\varepsilon - \mu_F)^2} \right] \quad (10)$$

$$\Theta(\varepsilon, i\omega_j) = [\omega_j Z(i\omega_j)]^2 + [\varepsilon - \mu_F + \chi(i\omega_j)]^2 + [\phi(i\omega_j)]^2$$

where

$$\lambda_{jj'}^{(\pm)} = \lambda(i\omega_j - i\omega_{j'}) \pm \lambda(i\omega_j + i\omega_{j'}) \quad (11)$$

are differences of the electron-phonon coupling parameter [11]. These equations are derived in Ref. [12].

C. cDOS μ^*

Combining both of the previously mentioned approximations leads to

$$Z(i\omega_j) = 1 + \frac{\pi k_B T}{\omega_j} \sum_{j'=-\infty}^{\infty} \frac{\omega_{j'} Z(\omega_{j'})}{\sqrt{\omega_{j'}^2 Z^2(\omega_{j'}) + \phi^2(i\omega_{j'})}} \lambda(i\omega_j - i\omega_{j'}) \quad (12)$$

$$= 1 + \frac{\pi k_B T}{\omega_j} \sum_{j'=0}^{\infty} \frac{\omega_{j'} Z(\omega_{j'})}{\sqrt{\omega_{j'}^2 Z^2(\omega_{j'}) + \phi^2(i\omega_{j'})}} \lambda_{jj'}^{(-)}$$

$$\phi(i\omega_j) = \pi k_B T \sum_{j'=-\infty}^{\infty} \frac{\phi(i\omega_{j'})}{\sqrt{\omega_{j'}^2 Z^2(\omega_{j'}) + \phi^2(i\omega_{j'})}} [\lambda(i\omega_j - i\omega_{j'}) - \mu^*] \quad (13)$$

$$= \pi k_B T \sum_{j'=0}^{\infty} \frac{\phi(i\omega_{j'})}{\sqrt{\omega_{j'}^2 Z^2(\omega_{j'}) + \phi^2(i\omega_{j'})}} [\lambda_{jj'}^{(+)} - 2\mu^*].$$

IV. SEMI-EMPIRICAL EQUATIONS FOR T_c

The McMillan equation [13] provides a direct but approximate method to calculate T_c based on empirically derived parameters. With small modifications done by Dynes [14], T_c is given by:

$$T_c^{\text{McM}} = \frac{\omega_{\log}}{1.2} \exp\left(-\frac{1.04(1 + \lambda)}{\lambda - \mu^*(1 + 0.62\lambda)}\right), \quad (14)$$

where the logarithmic average of the electron-phonon spectral function ω_{\log} and the electron-phonon coupling strength λ are defined as

$$\omega_{\log} = \exp\left(\frac{2}{\lambda} \int_0^{\infty} \frac{\alpha^2 F(\omega)}{\omega} \ln(\omega) d\omega\right), \quad (15)$$

$$\lambda = \int_0^{\infty} d\omega \frac{\alpha^2 F(\Omega)}{\omega}. \quad (16)$$

The expression for $\alpha^2 F(\Omega)$ is given in the main text Eq. (11), and μ^* is the semi-empirical Coulomb pseudopotential.

Allen and Dynes [15] added prefactors to optimize Eq. (14):

$$T_c^{\text{AD}} = f_1 f_2 T_c^{\text{McM}}, \quad (17)$$

with f_1 and f_2 defined by

$$f_1 = \left[1 + \frac{\lambda}{2.46} (1 + 3.8\mu^*)^{3/2} \right]^{1/3}, \quad (18)$$

$$f_2 = 1 + \frac{\left(\frac{\omega_2}{\omega_{\text{log}}} - 1 \right) \lambda^2}{\lambda^2 + \left[1.82(1 + 6.3\mu^*) \frac{\omega_2}{\omega_{\text{log}}} \right]^2}, \quad (19)$$

and ω_2 by:

$$\omega_2 = \frac{2}{\lambda} \int_0^\infty \alpha^2 F(\omega) \omega d\omega. \quad (20)$$

Eq. (17) was further improved using machine learning to get the following expression for a more accurate description, especially for high- T_c hydride superconductors [16]:

$$T_c^{\text{ML}} = f_\omega f_\mu T_c^{\text{McM}}, \quad (21)$$

with the prefactors

$$f_\omega = 1.92 \left[\frac{\lambda + \frac{\omega_{\text{log}}}{\omega_2} - \sqrt[3]{\mu^*}}{\sqrt{\lambda} \cdot \exp\left(\frac{\omega_{\text{log}}}{\omega_2}\right)} \right] - 0.08, \quad (22)$$

and

$$f_\mu = \frac{6.86 \exp\left(\frac{-\lambda}{\mu^*}\right)}{\frac{1}{\lambda} - \mu^* - \frac{\omega_{\text{log}}}{\omega_2}} + 1. \quad (23)$$

V. DERIVATION OF THE ELECTRON NUMBER EQUATION

A. Non-interacting electrons

In the case of non-interacting (NI) electrons, the electron number can be calculated via

$$\begin{aligned} N_e^{\text{NI}} &= 2 \int d\varepsilon N(\varepsilon) n_{\text{F}}(\varepsilon - \varepsilon_{\text{F}}) \\ &= \int d\varepsilon N(\varepsilon) \left[1 - 2k_{\text{B}}T \sum_{j=-\infty}^{\infty} \frac{\varepsilon - \varepsilon_{\text{F}}}{\omega_j^2 + (\varepsilon - \varepsilon_{\text{F}})^2} \right], \end{aligned} \quad (24)$$

where $N(\varepsilon)$ is the density of states per spin, n_{F} is the Fermi distribution function, and ω_j are the fermionic Matsubara frequencies. Even though both formulations are equivalent,

evaluating Eq. (24) through the Fermi function is numerically much more stable. At moderate temperatures, convergence is achieved almost immediately due to the sharp drop in the Fermi function. The summation however has to be truncated at some point, resulting in an additional error $S_{\text{tail}}^{\text{NI}}(\varepsilon, \varepsilon_{\text{F}})$

$$\begin{aligned}
2n_{\text{F}}(\varepsilon - \varepsilon_{\text{F}}) &= 1 - 2k_{\text{B}}T \sum_{j=-\infty}^{\infty} \frac{\varepsilon - \varepsilon_{\text{F}}}{\omega_j^2 + (\varepsilon - \varepsilon_{\text{F}})^2} \\
&= 1 - 2 \cdot 2k_{\text{B}}T \sum_{j=0}^{\infty} \frac{\varepsilon - \varepsilon_{\text{F}}}{\omega_j^2 + (\varepsilon - \varepsilon_{\text{F}})^2} \\
&= 1 - 4k_{\text{B}}T \sum_{j=0}^{\omega_j \leq \omega_c} \frac{\varepsilon - \varepsilon_{\text{F}}}{\omega_j^2 + (\varepsilon - \varepsilon_{\text{F}})^2} - \underbrace{4k_{\text{B}}T \sum_{\omega_j > \omega_c}^{\infty} \frac{\varepsilon - \varepsilon_{\text{F}}}{\omega_j^2 + (\varepsilon - \varepsilon_{\text{F}})^2}}_{:=S_{\text{tail}}^{\text{NI}}(\varepsilon, \varepsilon_{\text{F}})}.
\end{aligned} \tag{25}$$

Rearranging for the tail gives an estimate of the error

$$S_{\text{tail}}^{\text{NI}}(\varepsilon, \varepsilon_{\text{F}}) = 2n_{\text{F}}(\varepsilon - \varepsilon_{\text{F}}) - 1 + 4k_{\text{B}}T \sum_{j=0}^{\omega_j \leq \omega_c} \frac{\varepsilon - \varepsilon_{\text{F}}}{\omega_j^2 + (\varepsilon - \varepsilon_{\text{F}})^2}. \tag{26}$$

B. Superconducting phase

In the superconducting phase (SC), the number of electrons can be obtained through a generalization of Eq. (24):

$$N_{\text{e}}^{\text{SC}} = \int d\varepsilon N(\varepsilon) \left[1 - 2k_{\text{B}}T \sum_{j=-\infty}^{\infty} \frac{\varepsilon - \mu_{\text{F}} + \chi(i\omega_j)}{\theta(\varepsilon, i\omega_j)} \right], \tag{27}$$

where the denominator is defined as

$$\Theta(\varepsilon, i\omega_j) = [\omega_j Z(i\omega_j)]^2 + [\varepsilon - \mu_{\text{F}} + \chi(i\omega_j)]^2 + [\phi(\varepsilon, i\omega_j)]^2. \tag{28}$$

Splitting the sum again at ω_c and exploiting the fact that all self-energy components are even functions of ω_j gives an expression for the summation error:

$$\begin{aligned}
1 - 2k_{\text{B}}T \sum_{j=-\infty}^{\infty} \frac{\varepsilon - \mu_{\text{F}} + \chi(i\omega_j)}{\theta(\varepsilon, i\omega_j)} &= 1 - 2 \cdot 2k_{\text{B}}T \sum_{j=0}^{\infty} \frac{\varepsilon - \mu_{\text{F}} + \chi(i\omega_j)}{\theta(\varepsilon, i\omega_j)} \\
&= 1 - 4k_{\text{B}}T \sum_{j=0}^{\omega_j \leq \omega_c} \frac{\varepsilon - \mu_{\text{F}} + \chi(i\omega_j)}{\theta(\varepsilon, i\omega_j)} - \underbrace{4k_{\text{B}}T \sum_{\omega_j > \omega_c}^{\infty} \frac{\varepsilon - \mu_{\text{F}} + \chi(i\omega_j)}{\theta(\varepsilon, i\omega_j)}}_{:=S_{\text{tail}}^{\text{SC}}(\varepsilon, \mu_{\text{F}})}.
\end{aligned} \tag{29}$$

Above the Matsubara frequency cutoff ω_c , it is safe to assume that $Z(i\omega_j) = 1$, $\chi(i\omega_j) = 0$, $\phi^{ph}(i\omega_j) = 0$ and that the Coulomb contribution to the order parameter $\phi^c(\varepsilon) = 0$ can be

neglected. This allows us to approximate the superconducting tail by the non-interacting tail in Eq. (26) as a function of the Fermi level $S_{\text{tail}}^{\text{NI}}(\varepsilon, \varepsilon_{\text{F}}) \mapsto S_{\text{tail}}^{\text{NI}}(\varepsilon, \mu_{\text{F}}) \approx S_{\text{tail}}^{\text{SC}}(\varepsilon, \mu_{\text{F}})$ leading to:

$$\begin{aligned} 1 - 2T \sum_{j=-\infty}^{\infty} \frac{\varepsilon - \mu_{\text{F}} + \chi(i\omega_j)}{\theta(\varepsilon, i\omega_j)} &\approx 1 - 4k_{\text{B}}T \sum_{j=0}^{\omega_j \leq \omega_c} \frac{\varepsilon - \mu_{\text{F}} + \chi(i\omega_j)}{\theta(\varepsilon, i\omega_j)} + S_{\text{tail}}^{\text{NI}}(\varepsilon, \mu_{\text{F}}) \\ &= 2n_{\text{F}}(\varepsilon - \mu_{\text{F}}) - 4k_{\text{B}}T \sum_{j=0}^{\omega_j \leq \omega_c} \left[\frac{\varepsilon - \mu_{\text{F}} + \chi(i\omega_j)}{\theta(\varepsilon, i\omega_j)} - \frac{\varepsilon - \mu_{\text{F}}}{\omega_j^2 + (\varepsilon - \mu_{\text{F}})^2} \right]. \end{aligned} \quad (30)$$

Inserting this into Eq. (27) yields

$$N_{\text{e}}^{\text{SC}} = \int d\varepsilon N(\varepsilon) \left\{ 2n_{\text{F}}(\varepsilon - \mu_{\text{F}}) - 4k_{\text{B}}T \sum_{j=0}^{\omega_j \leq \omega_c} \left[\frac{\varepsilon - \mu_{\text{F}} + \chi(i\omega_j)}{\theta(\varepsilon, i\omega_j)} - \frac{\varepsilon - \mu_{\text{F}}}{\omega_j^2 + (\varepsilon - \mu_{\text{F}})^2} \right] \right\}, \quad (31)$$

which enables a more robust evaluation of the chemical potential. Based on numerical tests, this approach requires much lower Matsubara frequency cutoffs.

C. μ -update

When performing calculations within the variable DOS approximation, the conservation of electron number must be enforced by updating the chemical potential such that

$$f(\mu_{\text{F}}) = N_{\text{e}}^{\text{NI}} - N_{\text{e}}^{\text{SC}}(\mu_{\text{F}}) \stackrel{!}{=} 0 \quad (32)$$

is satisfied. $N_{\text{e}}^{\text{SC}}(\mu_{\text{F}})$ is a monotonic function of the chemical potential, guaranteeing a unique solution. However, monotonicity is easily violated when introducing a finite Matsubara frequency cutoff in the definition of N_{e}^{SC} . Using Eq. (31) instead of Eq. (27), ensures both faster convergence of the chemical potential and uniqueness of the root already at much lower cutoffs.

SUPPLEMENTARY REFERENCES

- [1] IsoME is available as a registered Julia package ([juliahub.com/ui/Packages/General/IsoME](https://github.com/ui/Packages/General/IsoME)), on GitHub (github.com/cheil/IsoME.jl), and Zenodo (DOI:10.5281/zenodo.14967551).
- [2] B. T. Matthias, T. H. Geballe, and V. B. Compton, *Rev. Mod. Phys.* **35**, 1 (1963).
- [3] C. Pellegrini and A. Sanna, *Nature Reviews Physics* **6** (2024).
- [4] A. L. Giorgi, E. G. Szklarz, E. K. Storms, A. L. Bowman, and B. T. Matthias, *Phys. Rev.* **125**, 837 (1962).
- [5] A. P. Drozdov, M. I. Erements, I. A. Troyan, V. Ksenofontov, and S. I. Shylin, *Nature* **525**, 73 (2015), publisher: Nature Publishing Group.
- [6] J. A. Flores-Livas, A. Sanna, and E. Gross, *The European Physical Journal B* **89**, 1 (2016).
- [7] P. Kong, V. S. Minkov, M. A. Kuzovnikov, A. P. Drozdov, S. P. Besedin, S. Mozaffari, L. Balicas, F. F. Balakirev, V. B. Prakapenka, S. Chariton, *et al.*, *Nature communications* **12**, 5075 (2021).

- [8] Y. Song, J. Bi, Y. Nakamoto, K. Shimizu, H. Liu, B. Zou, G. Liu, H. Wang, and Y. Ma, *Phys. Rev. Lett.* **130**, 266001 (2023).
- [9] C. Pellegrini, R. Heid, and A. Sanna, *Journal of Physics: Materials* **5**, 024007 (2022), publisher: IOP Publishing.
- [10] D. J. Scalapino, J. R. Schrieffer, and J. W. Wilkins, *Phys. Rev.* **148**, 263 (1966).
- [11] W. E. Pickett, *Physical Review B* **26**, 1186 (1982), publisher: American Physical Society.
- [12] H. Lee, S. Poncé, K. Bushick, S. Hajinazar, J. Lafuente-Bartolome, J. Leveillee, C. Lian, J.-M. Lihm, F. Macheda, H. Mori, H. Paudyal, W. H. Sio, S. Tiwari, M. Zacharias, X. Zhang, N. Bonini, E. Kioupakis, E. R. Margine, and F. Giustino, *npj Computational Materials* **9**, 1 (2023), publisher: Nature Publishing Group.
- [13] W. L. McMillan, *Phys. Rev.* **167**, 331 (1968).
- [14] R. C. Dynes, *Solid State Communications* **10**, 615 (1972).
- [15] P. B. Allen and R. C. Dynes, *Phys. Rev. B* **12**, 905 (1975).
- [16] S. R. Xie, Y. Quan, A. C. Hire, B. Deng, J. M. DeStefano, I. Salinas, U. S. Shah, L. Fanfarillo, J. Lim, J. Kim, G. R. Stewart, J. J. Hamlin, P. J. Hirschfeld, and R. G. Hennig, *npj Computational Materials* **8**, 14 (2022).